Bridging of Nonionic Reverse Micelles by a Myelin Transmembrane Protein

A. Merdas,[†] M. Gindre,[‡] J-Y. Le Huérou,[‡] C. Nicot,[‡] R. Ober,[§] W. Urbach,[||] and M. Waks*,[‡]

Laboratoire de Physique Statistique, URA 1302 CNRS, Ecole Normale Supérieure, 24 rue Lhomond, 75005 Paris, France; Laboratoire de la Matière Condensée, URA 792 CNRS, Collège de France, 10 Place Marcelin Berthelot, 75005 Paris, France; Laboratoire d'Imagerie Paramétrique, URA 1458 CNRS, Université Pierre et Marie Curie, 15 rue de l'Ecole de Médecine, 75006 Paris, France; and Laboratoire des Systèmes Moléculaires Organisés, Université René Descartes, 45 rue des Saints Pères, 75006 Paris, France

We have investigated the perturbation induced by a transmembrane protein in size, shape, and organization of reverse micelles, in a ternary system made of tetraethylene glycol monododecyl ether, dodecane, and water. The myelin proteolipid was solubilized in the micellar solution at high yield, preserving its α-helical structure. Characterization studies were carried out at a constant water-to-surfactant molar ratio of 13.7 and at a temperature of 31 °C, close to the L_α lamellar phase transition. Small-angle X-ray scattering experiments reveal that the shape of the protein-containing individual prolate micelles remains unchanged compared to protein-free micelles previously studied. The plot of ln $I(q)$ versus qR indicates an aggregation mechanism probably originating from intermicellar protein bridging. Dynamic light scattering measurements confirm attractive interactions between protein-containing micelles and provide the size of micelle–protein aggregates, which increases as a function of protein concentration. The hydrodynamic radius R_H varies from 290 to 450 Å when C, the protein-to-surfactant molar ratio, increases from 23×10^{-5} to 42×10^{-5}. Correlative variations of R_G, the radius of gyration measured by static light scattering, and of R_H for various values of C indicate that the novel structural arrangement is disk-oblate shaped and could be considered as a precursor of a protein-containing lamellar phase.

Introduction

The wide range of vital functions performed by biological membranes and membrane proteins has led investigators to the continuous search of systems susceptible to mimic, at least in part, the physical–chemical properties of the membrane architecture.[1] While such model systems may still lack much of the complexity of biological membranes, molecular assemblies of surfactant, water, and oil (micelles, lamelles, etc.), are able to capture a number of essential membrane features such as, among others, to maintain the functionally important interface between surfactant headgroups and sequestered water[2] and to solubilize proteins, preserving their conformational stability.[3] In particular, the monolayer structure of reverse micelles, where a number of physical–chemical parameters can be precisely controlled, has proved to constitute an excellent microenvironment for the study of membrane proteins.[4,5] Indeed from a perspective of membrane biophysics, monolayers can be considered as a simple structural model of one leaflet of a membrane basic structure.

In an earlier work, we have described the insertion mechanism of a transmembrane protein, the Folch-Pi proteolipid,[6] which is the major protein from the central nervous system myelin. Upon incorporation in reverse micelles of an anionic surfactant, sodium bis(2-ethyhexyl) sulfosuccinate (AOT), we have observed an increase of intermicellar interactions leading, in addition to aggregation phenomena, to a complex protein–micelle topology.[5] One of the questions addressed was to assess the relative importance of the surfactant and protein charge interactions in the insertion mechanism and to gain new insights into forces that stabilize the structure and the dynamics of a transmembrane protein within a bilayer. Such processes obviously play extremely important roles in protein design, engineering, and biocatalyst transformation.

To further these questions, we explored recently the properties of a ternary mixture composed of a nonionic surfactant tetraethylene glycol monododecyl ether ($C_{12}E_4$), dodecane, and water.[7] We described an isotropic, homogeneous phase existing above 29 °C, the transition temperature to the lamellar phase, and we determined the size and shape of the reverse micelles obtained at a definite water-to-surfactant molar ratio.

In this paper, we report that the same reverse micellar system solubilizes at 31 °C substantial amounts of the myelin proteolipid in a stable conformation with a high degree of periodic structure. We describe specific interactions occurring between the protein and the microemulsion, and we compare the size and shape characteristics of the protein-containing system to the protein-free one. We have used small-angle X-ray scattering and dynamic and static light scattering experiments to detect the novel structural arrangements induced by the protein and to explore the mechanisms involved. In particular, we show that, under the experimental conditions described here, prolate reverse micelles aggregate as a function of protein concentration to form large oblate ellipsoids. These findings imply that, in the nonionic surfactant studied, the micelle–macromolecule interaction has resulted in the modulation of physical parameters, which at a lower temperature allow the transition from the reverse micellar host system to the lamellar phase investigated previously by us.[8]

* To whom correspondence should be addressed.
[†] Université René Descartes.
[‡] Université Pierre et Marie Curie.
[§] Collège de France.
[||] Ecole Normale Supérieure.

Bridging of Nonionic Reverse Micelles

J. Phys. Chem. B, Vol. 102, No. 3, 1998 **529**

Material and Methods

Chemicals. Tetraethylene glycol monododecyl ether NIKKOL BL-4SY (denoted $C_{12}E_4$) was obtained from Nikko Chemicals Co. Ltd. (Tokyo, Japan). Anhydrous dodecane was purchased from Aldrich Chemical Co. (Milwaukee, WI) and isooctane Pro Analysi grade from Merck (Darmstadt, Germany). All other materials were from the highest purity grade available.

Protein Purification and Incorporation. The Folch-Pi proteolipid was purified from bovine brain as described elsewhere.[9] A slight modification was carried out as follows: after the first isooctane precipitation in a preweighed vessel, the proteolipid was suspended in an excess of dodecane sufficiently large to remove all the remaining traces of isooctane; it was then spinned at 3500 rpm at 4 °C for 10 min. We have shown that, under the above experimental conditions, 10−12 lipids remain tightly bound to one protein molecule; thiol groups are preserved as well as the thioester linkage between thiols and six fatty acid molecules.[9] The solubilization of the proteolipid was carried out at 31 °C by adding a weighed amount of the ternary mixture components to the precipitate. A few minutes of sonication at that temperature results in an isotropic, optically clear solution, ready for spectroscopic measurements.

Sample Preparation. All samples were prepared at 31 °C and at a single molar ratio of water-to-surfactant expressed as $W_0 = [H_2O]/([C_{12}E_4] − [C_{12}E_4]_{cmc}) = 13.7$. Since in reverse micelles the critical microemulsion concentration $[C_{12}E_4]_{cmc}$ at which micelles begin to form is higher than 10 mmol/L, dilution had to be carried out with the continuous phase solvent containing the surfactant at the cmc, so as to maintain the solution equilibrium without removing the surfactant from the micelles. Full experimental details are given in ref 7. Such dilutions have been performed on protein micellar solutions at a defined protein-to-surfactant molar ratio C and at a micellar volume fraction Φ ranging from 0.1 to 0.03: this procedure ensures that C and W_0 are kept constant during the experimental procedures.

Spectroscopic Measurements. The precise amount of protein incorporated in the micellar solution was determined from absorption measurements on a Cary model 118 spectrophotometer, thermostated at 31 °C. The molar extinction coefficient of the proteolipid was found to be identical with that measured previously (4.05×10^4 at 278 nm for a molecular weight of 30 000). The absorption of the protein-free ternary mixture is negligible in the ultraviolet 250−280 nm range. Corrected fluorescence emission spectra were also recorded at 31 °C on a Hitachi 4010 spectrofluorimeter after baseline subtraction and at a 3−5 nm bandwidth. Circular dichroism spectra were carried out on a computer-controlled Jouan MARK V dichrograph. Spectra were repetitively scanned in a 0.01 cm cell, averaged, baseline corrected, and converted to mean residue ellipticities $[\theta]$.

Small-Angle X-ray Scattering (SAXS). Samples were filled at 31 °C in Lindeman capillaries of 1 mm diameter and sealed. The X-ray generator was a copper rotating anode machine operating at 40 kV and 25 mA. The X-ray apparent source had dimensions 0.1 mm × 0.1 mm. A vertical mirror acts as a total reflector for the $\lambda_{K\alpha} = 1.54$ Å wavelength, eliminates shorter wavelengths of the beam, and directs the X-rays on the positive proportional counter. A nickel filter attenuates the $K\beta$ waves. The dimensions of the beam on the counter are 3 mm vertically and 0.3 mm horizontally. The counter has a window of 3 mm height, a 50 mm useful length, and a 200 μm spatial resolution. The distance between the sample and the counter is 802 mm.[10] The SAXS data are analyzed using the general equation for the scattered intensity derived by Guinier and Fournet[11] as described in ref 7.

From the intensity $I(q)$ the pair distribution function $p(r)$, which is the distance histogram of the particle, is obtained by[12]

$$p(r) = \frac{1}{2\pi^2}\int_0^\infty I(q)qr\,\sin(qr)\,\mathrm{d}q \tag{1}$$

where q is the scattering wave vector.

Dynamic Quasi-Elastic Light Scattering (DQLS). The experiments were performed using a laboratory-built autocorrelator. The autocorrelation function was measured in 105 points grouped in four zones with different sampling times. This allows a precise determination of both short time and asymptotic behavior of the autocorrelation function in the same run. The correlator was interfaced to a computer allowing the continuous control of the baseline. Due to the low scattering power of some samples, occasional dust particles can seriously disturb the results. This problem was solved by introducing a check procedure: at the end of each run the baseline was calculated and compared to the value measured in the last channel. If the discrepancy was $>5 \times 10^{-3}$ of the signal amplitude, the data were rejected; if the discrepancy was under that value, the data were stored in the computer. At least 100 runs per experiment were collected. The autocorrelation function of scattered intensity was fitted with the following expression:

$$\langle I(t)\,I(t+\tau)\rangle = 1 + k\mathrm{e}^{-2t/\tau} \tag{2}$$

where $\tau^{-1} = D_c q^2$.[13] D_c is the collective diffusion coefficient, and q the scattering wave vector is given by

$$q = \frac{4n\pi}{\lambda}\sin\!\left(\frac{\theta}{2}\right) \tag{3}$$

where n is the refractive index of the sample and λ is the wavelength of the incident light (5145 Å). The scattering angle θ was varied between 30° and 150°. In all the samples studied a two-exponential fit was attempted, where two characteristic times τ_1 and τ_2 ($\tau_2 \ll \tau_1$) scale as q^{-2}.

Static Light Scattering. In the absence of interparticle interactions, a comparison of the scattering intensity $I(q)$ at low and intermediate q ranges, incorporating calculated intensities of a simple model, can give valuable indications on the structure of aggregates present in a solution.

For $qR_G < 1$, the intensity $I(q)$ can be written as follows:

$$I(q) \approx 1 - \frac{q^2}{3}R_G{}^2 + ... \tag{4}$$

where R_G is the radius of gyration of the micellar objects. Although it is possible to measure directly $I(\theta)$ as function of θ, such measurements are complicated by slow drifts in the incident light intensity. This complication can be circumvented by measuring the dissymmetry function $\mathrm{d}\theta$, defined in eq 5, as the ratio of the intensity of light scattered at complementary angles θ and $180° − \theta$.

$$\mathrm{d}\theta = \frac{I(\theta)}{I(\pi - \theta)} \tag{5}$$

From eqs 4 and 5 one obtains

$$\mathrm{d}\theta \approx 1 + \left(\frac{4\pi n}{\lambda}\right)^2\!\left(\frac{R_G{}^2}{3}\right)\cos(\theta) \tag{6}$$
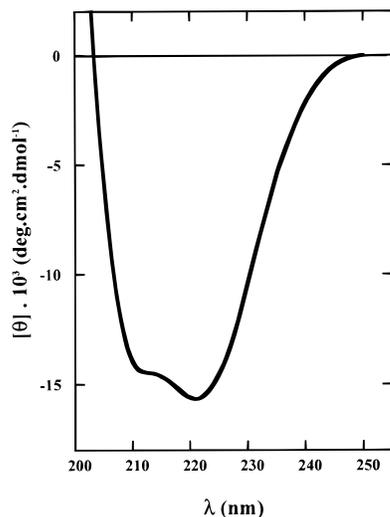
Figure 1. Far-UV circular dichroism spectrum of the myelin proteolipid in a micellar solution at a water-to-surfactant molar ratio $W_0 = 13.7$. The protein-to-surfactant molar ratio C is 8.6×10^{-5}, the micellar volume fraction $\Phi = 0.14$, and the temperature is 31 °C. $[\theta]$ represents the mean residue ellipticity in deg cm^2 dmol^{-1}.

From eq 6 a plot of $d\theta$ as function of $\cos(\theta)$ at low q yields a straight line, where the slope is a function of R_G. Deviation in the linear dependence of $d\theta$ becomes appreciable for R_G values higher than 600 Å.[14]

Results and Discussion

Among the many systems investigated, three-component mixtures of the type nonionic surfactant, H$_2$O, oil have attracted our attention because of their versatile phase composition. They self-organize into a large array of well-documented phases (isotropic, multilamellar, cubic, etc.), experimentally delineated by the weight fraction of their components, as well as by temperature variation.[15] We have previously explored the oil-rich corner of the ternary system C$_{12}$E$_4$, dodecane, and H$_2$O phase diagram.[7] We have characterized a fluid, isotropic, optically transparent phase existing at a temperature just above the lamellar phase. At 31 °C and at a W_0 value of 13.7, the particles behave as spherocylindrical micelles of radius 44 ± 2.5 Å, an asymmetry of 6 ± 2, and a hydrodynamic radius, R_H, in the 115−120 Å range. In this report, we compare under the same experimental conditions the characteristics of identical micellar solutions, after myelin proteolipid insertion.

Spectroscopic Measurements: Protein Insertion. The myelin protein was solubilized as a lipid−protein complex (proteolipid) in order to preserve its conformational integrity.[9] As judged from the ultraviolet absorption spectrum recorded from 450 to 240 nm (not shown), substantial amounts (4.2×10^{-4} M) of the proteolipid are fully dissolved, with minimal scattering. Interestingly, in reverse micelles of an anionic surfactant (AOT), water, and isooctane,[5] we have reported previously a much lesser solubility of the proteolipid (1.5×10^{-4} M).

Circular dichroism spectra were easily recorded from 250 to 200 nm, due to the very low absorption of the liquid mixture in the far-UV. Figure 1 illustrates a typical far-UV CD spectrum indicative of a structure that is substantially α-helical. At 222 nm, the ellipticity value is −16 000 deg cm^2 dmol^{-1}, and calculations[16] yield a value of about 55% α-helix, the remaining being random with a small content in β-pleated sheet and bends. Although we do not yet know the three-dimensional structure of the Folch-Pi proteolipid in myelin, the measured conformation is compatible with the most recently proposed models of the
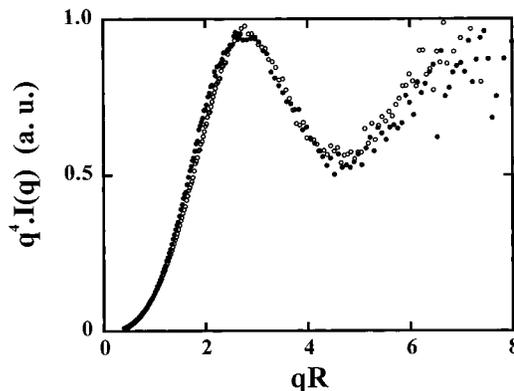

Figure 2. X-ray scattering curves at 31 °C. Comparison of experimental data at $\Phi = 0.06$ for protein-containing (●) at $C = 77 \times 10^{-5}$ and protein-free (○) micelles. $q^4 I(q)$ is plotted versus qR (R is the spherocylinder radius). Both curves are normalized to the same maximal value.

protein, displaying four transbilayer α-helices as obtained from theoretical considerations and chemical experiments.[17] The insertion of the membrane protein into a nonionic as well as an ionic surfactant system[18] leads to very close conformations. This result is confirmed by fluorescence emission spectra (not shown), which display a maximum at 332 nm (after excitation at 295 nm), indicating that tryptophan fluorophores are shielded from water.

Micellar Shape and Size. *SAXS Experiments.* They were performed at a high protein-to-surfactant molar ratio $C = (77 ± 5) \times 10^{-5}$ and compared to the same experiments carried out with protein-free micellar solutions, at several values of Φ, the micellar volume fraction. Figure 2 shows the plot of $q^4 I(q)$ versus qR, where R represents the cylinder radius obtained from the fit. The two curves can be superposed (with R(protein-containing micelle)/R(protein-free micelle) = 0.85), indicating an identical shape for both particles. Furthermore, the observation of relative positions of the maximum q(max) and of the minimum q(min) in the curve $q^4 I(q)$ vs q allows to discriminate between the two shapes: prolate or oblate. We found for $x = q$(min)/q(max) a value around 1.7. This value is close to that of a prolate (∼1.8) but far from that of an oblate (∼2.0). From the Porod regime we can therefore conclude that the particles observed by SAXS are prolate but not oblate shaped.

In Figure 3, we show the semilog plot of the same results. At low qR values, the curve obtained with protein-containing micelles displays deviation from that obtained for protein-free micelles. It suggests clearly attractive interactions between micelles induced by the protein. To gain additional information on the aggregation of the particles, the pair distribution function for protein-containing micelles was computed from the measured values of $I(q)$. The $p(r)$ curve vs r is compared in Figure 4 to the same curve obtained previously in the absence of the protein.[7] The presence of a double bump in the $p(r)$ function, induced by the insertion of the transmembrane protein, is obvious and has been interpreted according to Glatter[12] as characteristic of associated micelles (here by a protein). Note that $p(r)$ obtained for large values of r is very sensitive to $I(q)$ measured for q tending to 0 and depends thus strongly on intermicellar correlations, including additional correlations induced by the protein itself [$S(q)$ deviates from 1]. The maximal value of r (the large dimension) will be therefore obtained with a high uncertainty. Thus, protein incorporation does not lead to differently shaped micelles; individually they retain their original shape and a small axis of a comparable magnitude, while forming aggregates.
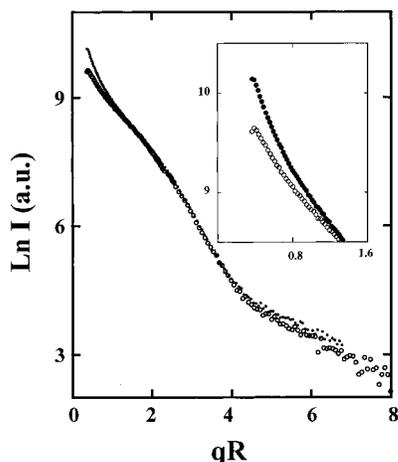
Bridging of Nonionic Reverse Micelles

J. Phys. Chem. B, Vol. 102, No. 3, 1998 **531**

Figure 3. Plot of ln $I(q)$ versus qR. Comparison of experimental data at 31 °C for protein-containing (●) at $C = 77 \times 10^{-5}$ and protein-free reverse micelles (○); $\Phi = 0.06$. The inset gives credence to the attractive interactions induced by the protein between micelles within an aggregate.
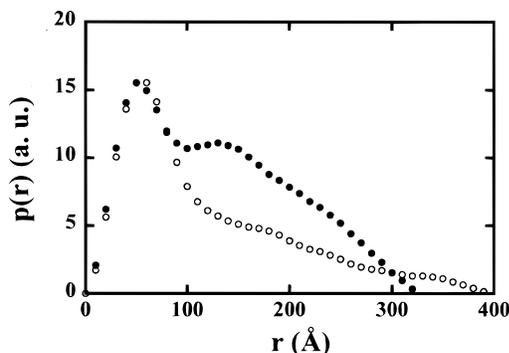

Figure 4. Pair distribution function $p(r)$ obtained from $I(q)$ using eq 1 at $\Phi = 0.06$ for protein-containing (●) at $C = 77 \times 10^{-5}$ and for protein-free micelles (○). Note in the former curve the presence of a double bump characteristic of associated micelles (ref 12).

Light Scattering. DQLS and angular dissymmetry measurements were simultaneously performed on the same protein-containing micellar solutions. Experiments were done at three different protein-to-surfactant molar ratios: $C = 23 \times 10^{-5}$, 30.5×10^{-5}, and 42×10^{-5} (lower than that measured by X-ray scattering). Dynamic light scattering is a global measurement taking into account both protein-free and protein-containing micelles. At the protein concentrations studied, the results can be fitted by a bimodal distribution, differing in τ, the time constant, by a factor of 3 and represented in Figure 5 where τ^{-1} is plotted versus q^2. The variation of the diffusion coefficient (D_c) as a function of the micellar volume fraction is illustrated in Figure 6. The higher diffusion coefficients agree, within the experimental uncertainty, to the value extrapolated to $\Phi \rightarrow 0$ previously found for the protein-free micelles: $D_0 = 1.5 \times 10^{-7}$ cm^2 s^{-1}. The lower diffusion coefficients obtained for protein-filled micelles decrease with protein concentration. The lowest value ($D_0 = 0.33 \times 10^{-7}$ cm^2 s^{-1}) corresponds to the highest protein-to-surfactant molar ratio, implying the formation of large aggregates, probably by protein–micelle close interactions. The values of D_0 and R_H, the hydrodynamic radius, extrapolated to zero micellar volume fraction are summarized in Table 1.

As a matter of comparison, it is interesting that, at the highest C value measured in AOT reverse micelles (7.5×10^{-5}), the mean R_H value obtained is much higher (1300 Å) than that measured in C$_{12}$E$_4$ micelles (450 Å for $C = 45 \times 10^{-5}$).
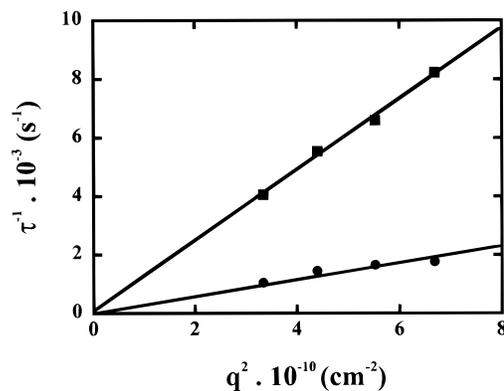

Figure 5. Dynamic light scattering experiments at 31 °C. The diffusion coefficients D_c are deduced by fitting the light scattering curve by two exponential functions with two characteristic times τ scaling as q^{-2}. Protein-free (■) and protein-containing (●) micelles at $C = 23 \times 10^{-5}$; $\Phi = 0.05$. The two respective diffusion coefficients are obtained from the slope.
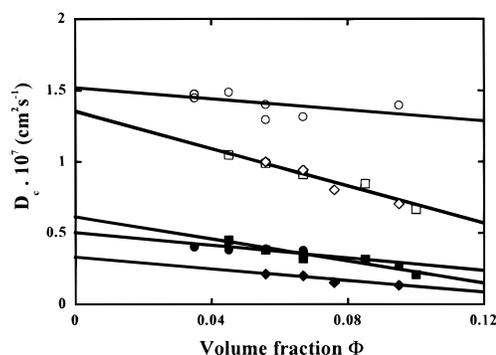

Figure 6. Variation of D_c as a function of Φ, the micellar volume fraction, at different protein-to-surfactant molar ratios C at 31 °C. The open and filled symbols represent respectively protein-free and protein-containing reverse micelles. $C = 23 \times 10^{-5}$ (□), $C = 30 \times 10^{-5}$ (○), and $C = 42 \times 10^{-5}$ (◇).

TABLE 1: Micellar Size Parameters

C^a	$D_0 \times 10^7$ (cm^2 s^{-1})^d		R_H (Å)^e		R_G (Å)
	b	c	b	c	
23.0	1.52	0.59	110 ± 10	290 ± 20	307 ± 30
30.5	1.44	0.50	104 ± 10	330 ± 20	340 ± 34
42.0	1.52	0.34	110 ± 10	450 ± 25	500 ± 20

^{a} $C = $ [protein]/[C$_{12}$E$_4$] $\times 10^5$. ^{b} Protein-free micelles. ^{c} Protein-containing micelles. ^{d} D_0 is D_c extrapolated to $\Phi \rightarrow 0$. ^{e} R_H, the hydrodynamic radius, is obtained from the Stokes−Einstein relation $D_0 = kT/6\pi\eta R_H$; R_G is the gyration radius.

Angular dissymmetry measurements allow the determination of the radius of of gyration (R_G) of the aggregated micelles. In our experiments protein-free micelles do not interfere with the measurements of protein-filled micelles, which associate to form large aggregates. The plots of the dissymmetry function dθ vs cos(θ) obtained at three different protein-to-surfactant molar ratios are illustrated in Figure 7. The increase of the slope with protein concentration is indicative of the increase of the radius of gyration of the aggregates as shown in Table 1. Apparently, no dependence of R_G with the micellar volume fraction Φ was observed under these experimental conditions. The fact that R_G is independent of Φ whereas D_c is dependent on it may look surprising at first glance. A detailed explanation of this apparent contradiction is presented in note 19.

Because of the complexity of the results originating from the perturbation of the system induced by protein incorporation, we have thought that, from the value of the hydrodynamic radius
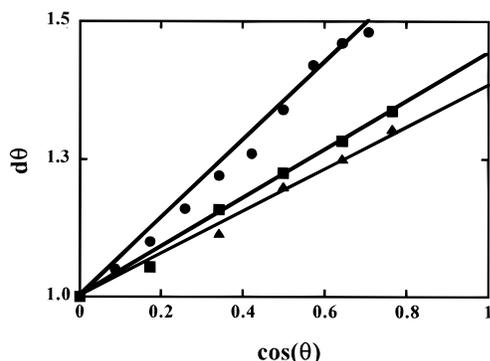
Figure 7. Plots of dissymmetry dθ versus cos(θ) carried out at 31 °C at different protein-to-surfactant molar ratios $C = 23 \times 10^{-5}$ (▲), $C = 30 \times 10^{-5}$ (■), and $C = 42 \times 10^{-5}$ (●) at $\Phi = 0.05$.
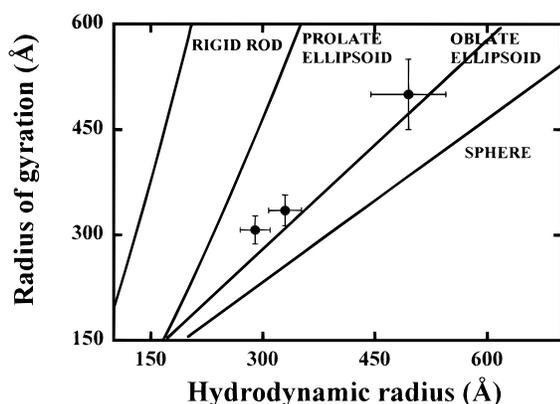

Figure 8. Correlative variations of R_G, the gyration radius, with R_H, the hydrodynamic radius, of aggregates. Solid lines show the theoretical predictions for rods, prolate, oblate ellipsoids, and spheres, calculated using for the smaller geometrical parameter the radius obtained from SAXS experiments (see text and note 19).

alone, we would be unable to deduce properly the shape of the protein-containing aggregates. Different shapes displaying the same value of R_H will obviously yield different values for R_G. Thus, different types of relationships will exist between R_H and R_G depending on the shape of the aggregates.[14]

The plot of R_G vs R_H, along with those of different geometrical models such as spheres, rigid rods, prolate, or oblate ellipsoids, allows to distinguish between the possible shapes of the aggregates. We have used the equations of Perrin[20,21] for the theoretical curves of the models, assuming that the smaller geometrical parameter represents the mean radius[7] of the spherocylindrical protein-free micelle (44 Å), i.e., the radius obtained from Figure 2 after addition of the surfactant tail length (8 Å). Such a plot is illustrated in Figure 8, showing that the large protein-containing aggregate can be best fitted by an oblate ellipsoid (disklike shape), the low dissymmetry observed ruling out a rodlike shape. In contrast, for AOT reverse micellar aggregates, the best fit corresponded to a different structure, a random coil.[5]

Structural Features of the Protein-Containing Micelles. The incorporation of a transmembrane protein into a self-assembled and well-characterized ternary system may result in overall structures that differ significantly from the initial ones.[8] In this work, we have inserted into nonionic reverse micelles a transmembrane protein (more precisely a water-insoluble protein–lipid complex) modeled in native myelin as a hydrophobic core comprised between two opposite hydrophilic domains.[22] This structure implies that in micelles the protein can sample two different types of environments: on one hand, the micellar
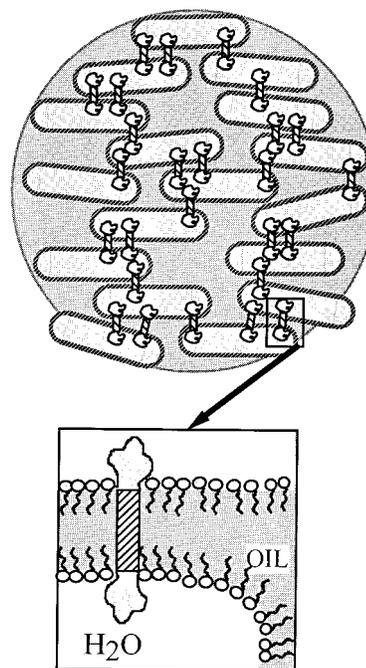

Figure 9. Cartoon illustrating an artist's view of aggregated prolate micelles, linked by protein molecules and aggregated as a disk. It is assumed that micelles are organized as a single layer. The view is perpendicular to the layer plane. The inset illustrates the bilayer structure assembled by the protein bridging two inverted micelles. (Other models may also be equally acceptable.)

aqueous core in contact with the surfactant polar headgroups and, on the other, the hydrocarbon phase with the protruding surfactant hydrophobic tails. The most straightforward topology and the most stable orientation of these protein segments can be represented as follows:[23] the two opposed hydrophilic segments are in contact with the water pool of two distinct micelles, linked by the bundle of four hydrophobic α-helixes immersed in dodecane and in contact with the surfactant tails.[5] Thus, one or several protein molecules may bring together and bridge the monolayers of two different inverted micelles, reconstituting a bilayer (Figure 9). In addition, the substantial presence of $C_{12}E_4$ monomers in the mixture suggests the possible binding of a significant number of them to the hydrophobic α-helical bundle, thus facilitating the solubility of the protein.

From SAXS measurements we know that the presence of the protein does not modify the shape of the individual micelles, although it promotes an aggregation between them. The decrease of the prolate small axis by a 0.85 factor is consistent with the location of a protein domain at the polar–apolar interface, leading to an area increase of that interface for a constant water volume. As a consequence, the number of micelles will increase while their small axis decreases. From light scattering measurements, we observe an increase of the aggregate size with protein concentration, yet even at the highest protein concentration measured, protein-free micelles can be observed in substantial amounts. Assuming a spherocylindrical shape for these micelles, geometric considerations lead to a mean surfactant aggregation number of ∼2500. It can be then calculated that for $C = 42 \times 10^{-5}$ the ratio of protein molecules to micelles is close to 1. But since we still observe a significant number of protein-free micelles at that protein concentration, we can assume that, in the aggregates formed between micelles and protein, several protein molecules are involved in the bridging of neigboring micelles (represented in the cartoon in Figure 9), leaving a number of micelles protein-free.

If we remember that experiments are carried out near the transition temperature to the L_α phase, it is conceivable that micelles floating in dodecane tend to organize themselves in such a way that incorporation of the protein will stabilize oblate aggregates. These aggregates may display a thickness of the same order of magnitude as the initial micellar radius. The micellar solution may thus constitute the precursor of the L_α phase, taking place at 29 °C.

Our present findings are consistent with the picture (but do not prove) that above 29 °C the protein is already inserted between two surfactant micellar monolayers. When the temperature is lowered, the protein has to migrate by lateral diffusion, along the monolayers, creating a stable structural network of minimum energy as reported elsewhere.[8] In the absence of surfactant charges, the suggested mechanism of such a complex organization probably originates essentially from hydrophobic forces.[24]

Conclusion

We have described herein a ternary system (nonionic surfactant−oil−water) susceptible to solubilize transmembrane proteins in high yield, under a nondenatured stable conformation, in the absence of surfactant charges.[25] Whether the characteristics of the system observed in this work constitute a general property of membrane proteins or are linked to the "zipperlike" function of the Foch-Pi proteolipid in myelin[26] remains to be investigated. Nevertheless, native myelin is a charged membrane composed of several different types of lipids, most of them bearing negative charges. Since we have solubilized in a previous work[5] the membrane protein in negatively charged reverse micelles (AOT, isooctane, and water), we would like at this point to summarize the similarities and differences observed in the behavior of the two systems.

In both systems, the amphipatic environment of the proteolipid is an important determinant in the folding and maintenance of an identical membrane protein structure. However, the higher yield obtained in the solubilization of the basic proteolipid in the nonionic reverse micellar system indicates that the sulfonate negative charges of the surfactant are not a prerequisite for protein incorporation and that hydrophobic interactions are the driving forces in the solubilization mechanism.

In contrast to the present organization of the oblate protein−micelle clusters, we have observed in the ionic surfactant system the appearance of long-sized random coils, even at very low C ratio. This finding emphasizes the role of the attractive interactions between the anionic surfactant and the positively charged protein, resulting finally in the precipitation of aggregates with further increase of C, the protein-to-surfactant ratio.[5]

We can therefore conclude that the complex arrangement induced by the membrane protein in nonionic micelles seems to possess the main features required for a stable structure on the way of the micelle−lamellar phase transition.

References and Notes

(1) Fendler, J. *Membrane Mimetic Chemistry*; John Wiley and Sons: New York, 1982; Chapter 10.

(2) Luisi, P. L.; Magid, L. J. *Crit. Rev. Biochem.* **1986**, *20*, 409.

(3) Nicot, C.; Waks, M. *Biotechnol. Genet. Eng. Rev.* **1995**, *13*, 267.

(4) Nicot, C.; Vacher, M.; Vincent, M.; Gallay, J.; Waks, M. *Biochemistry* **1985**, *24*, 7024.

(5) Binks, B. P.; Chatenay, C.; Nicot, C.; Urbach, W.; Waks, M. *Biophys. J.* **1989**, *55*, 949.

(6) Lees, M. B.; Brostoff, S. W. *Myelin;* Morell, P., Ed.; Plenum Press: New York, 1984; Chapter 6.

(7) Merdas, A.; Gindre, M.; Ober, R.; Nicot, C.; Urbach, W.; Waks, M. *J. Phys. Chem.* **1996**, *100*, 15180.

(8) Nicot, C.; Waks, M.; Ober, R.; Gulik-Krzywicki, T.; Urbach, W. *Phys. Rev. Lett.* **1996**, *77*, 3485.

(9) Vacher, M.; Waks, M.; Nicot, C. *J. Neurochem.* **1989**, *52*, 117.

(10) Giasson, S.; Espinat, D.; Palermo, T.; Ober, R.; Pessah, M.; Morizur, M. F. *J. Colloid Interface Sci.* **1992**, *153*, 355.

(11) Guinier, A.; Fournet, G. *Small Angle Scattering of X-Rays;* John Wiley and Sons: New York, 1955; Chapter 6.

(12) Glatter, O. *J. Appl. Crystallogr.* **1979**, *12*, 166.

(13) Koppel, D. E. *J. Chem. Phys.* **1972**, *57*, 4814.

(14) Young, C. Y.; Missel, P. J.; Mazer, N. A.; Benedek, G. B.; Carey, M. C. *J. Phys. Chem.* **1978**, *82*, 1375.

(15) Kahlweit, M.; Strey, M.; Haase, D.; Kunieda, H.; Schmeling, T.; Faulhaber, B.; Borkovec, M.; Eicke, H.-F.; Busse, G.; Eggers, F.; Funck, T. H.; Richmann, H.; Magid, L.; Söderman, O.; Stilbs, P.; Winkler, J.; Dittrich, A.; Jahn, W. *J. Colloid Interface Sci.* **1987**, *118*, 436.

(16) Chen, Y. H.; Yang, J. T.; Chau, K. H. *Biochemistry* **1974**, *13*, 3350.

(17) Weimbs, T.; Stoffel, W. *Biochemistry* **1992**, *31*, 12289.

(18) Delahodde, A.; Vacher, M.; Nicot, C.; Waks, M. *FEBS Lett.* **1984**, *172*, 343.

(19) The fact that D_c is dependent on Φ, the micellar volume fraction, while R_G is independent is explained by the following equations. According to Benoit et al. (*J. Phys. Chem.* **1954**, *58*, 635), one can define the apparent gyration radius as

$$R_G{}^{app} \approx R_G(1 + B\phi) \tag{1}$$

where B, the second virial coefficient, is ≤ 0 in our system of aggregates. On the other hand, one obtains from DLS

$$D_c = D_0(1 + k_1\phi + ...)(1 + B\phi + ...)$$
$$\approx D_0(1 + \phi(k_1 + B) + ...) \tag{2}$$

where $k_1 < 0$ in accordance with Carter and Phillies (*J. Phys. Chem.* **1985**, *89*, 5118). Since in this system B is ~ 0 and k_1 is negative, the variation of D_c with Φ is larger than that of R_G which seems therefore concentration independent.

(20) Perrin, J. *J. Phys. Radium* **1936**, *7*, 1.

(21) Van De Sande, W.; Persoons, A. *J. Phys. Chem.* **1985**, *89*, 404.

(22) Popot, J. L.; Pham Dinh, D.; Dautigny, A. *J. Membr. Biol.* **1991**, *120*, 233.

(23) Ben-Tal, N.; Honig, B. *Biophys. J.* **1996**, *71*, 3046.

(24) Kauzmann, W. *Adv. Protein Chem.* **1959**, *14*, 1.

(25) Honig, B.; Nicholls, A. *Science* **1995**, *268*, 1144.

(26) Klugmann, M.; Schwab, M. H.; Pühlhofer, A.; Schneider, A.; Zimmermann, F.; Griffiths, I. R.; Nave, K. A. *Neuron* **1997**, *18*, 59.